Research Article | Vol. 12, No. 11 / 1 Nov 2021 / Biomedical Optics Express 6686

Biomedical Optics EXPRESS

Fast diffuse correlation spectroscopy with a low-cost, fiber-less embedded diode laser

ARINDAM BISWAS,[1,*] SADHU MOKA,[1] ANDREAS MULLER,[2] AND ASHWIN B. PARTHASARATHY[1]

[1]Department of Electrical Engineering, University of South Florida, 4202 E. Fowler Avenue, ENG030, Tampa, FL 33620, USA
[2]Department of Physics, University of South Florida, 4202 E. Fowler Avenue, ISA2019, Tampa, FL 33620, USA
*abiswas@usf.edu

Abstract: Diffuse correlation spectroscopy (DCS), a popular optical technique for fast noninvasive measurement of blood flow, is commonly implemented using expensive fiber-coupled long coherence length laser systems. Here, we report the development of a portable and fiber-less approach that can be used as a low-cost alternative to illuminate tissue in DCS instruments. We validate the accuracy and noise characteristics of the fiber-less DCS laser source, by comparisons against traditional DCS light sources, with experiments on controlled tissue-simulating phantoms and in humans.

1. Introduction

Blood is a carrier of essential nutrients and oxygen to tissues in human body and quantitative measurement of blood flow provides vital information about tissue health, viability and disease states [1–6]. Over the past few decades, Diffuse Correlation Spectroscopy (DCS) [7–9] has emerged as a popular optical method to quantitatively and noninvasively measure blood flow in the clinic. DCS has been validated against a variety of 'gold-standard' blood flow measurement techniques [10–13], and its utility has been demonstrated in clinical blood flow measurements in the adult brain [8,9], pediatric brain [12,14], muscle [4,10] and spinal cord [15,16]. A typical DCS instrument uses light from lasers with long coherence length to illuminate tissue through long fiber optic cables. Fiber optic cables also collect and direct diffusely reflected light, a few centimeters away from the illumination position on the tissue surface, to photon-counting avalanche photo diode modules for detection. The use of these lasers and detection systems results in a relatively expensive and bulky instrument, especially when compared to more commercial and ubiquitous optical sensors based on Near Infrared Spectroscopy (NIRS). We and others have recently made several technical improvements to the detection and processing of DCS photon counts that have resulted in simpler and faster instruments. These include fast software autocorrelators [17,18] and fast field programmable gate arrays/microcontrollers [19,20] for measuring pulsatile blood flow, as well as new detection systems based on CCD cameras [21–23], multipixel Silicon Avalanche Photodiode (SPAD) arrays [24] and single photo diodes [25,26]. However, the need to use heavy/bulky laser systems limit the portability of DCS instruments. In this contribution, we report the development of a small, portable, fiber-less laser illumination system that can be directly embedded into DCS measurement probes.

In DCS, estimates of blood flow are derived from diffusion-based analysis of the autocorrelation of *coherent* fluctuations in light intensity backscattered from the tissue surface [8, 27,28]. Consequently, the phase coherence of the scattered field is an important factor in the design of DCS instruments/light sources [28–30]. Diffusion theory and Monte Carlo simulations of light transport [31] have shown that the minimum coherence length for DCS light sources must be greater than the width of the pathlength distribution of photon travel in tissue – estimated to

#435136 https://doi.org/10.1364/BOE.435136
Journal © 2021 Received 24 Jun 2021; revised 20 Sep 2021; accepted 21 Sep 2021; published 4 Oct 2021
Corrected: 11 Oct 2021

Biomedical Optics EXPRESS

be five to ten times the source-detector separation [7,31] (*e.g.,* 100 mm for a source-detector separation of 10 mm). Nevertheless, since DCS instruments typically utilize long fiber optic cables, laser sources with significantly longer coherence lengths (~50 m) need to be used, in order to compensate for additional length of photon travel through the fiber [8,17]. Given that the coherence requirement is significantly lower than the laser sources traditionally used for DCS measurements, a light source with relatively low coherence length could help simplify the instrumentation, enable wearable designs, reduce system cost and power consumption. In this study, we have designed one such small-form factor laser system, which we term fiber-less DCS (FBDCS) using a single mode laser diode (coherence length ~3.72 m) with a collimating lens to couple light directly to the tissue surface, eliminating need for coherence length overhead introduced by long fiber optic cables. In tissue simulating phantoms and *in-vivo* experiments, we show that the FBDCS light source compares favorably with fiber-coupled wavelength stabilized laser sources traditionally used in DCS, in terms of the accuracy and fidelity of estimated blood flow indices, but also in terms of the signal-to-noise ratio of measured intensity autocorrelation functions,

2. Theory

2.1. Diffuse correlation spectroscopy (DCS)

We briefly review the principles behind DCS and direct the reader to several excellent reviews on the topic for a more comprehensive discussion [7–9,27]. In DCS, tissue is illuminated by light from a coherent laser source, and the backscattered light, which has diffused through tissue, is collected and recorded a few centimeters away from the source on the tissue surface. The detected intensity is the interference of light travelling through several pathlengths in tissue; interaction of these light pathlengths with moving particles (*i.e.,* red blood cells) result in temporal fluctuations in the intensity, which are analyzed to estimate blood flow. Formally, the dynamics of temporal intensity fluctuations ($I(t)$) are quantified as a normalized temporal autocorrelation function $g_2(\tau)$ [7]–

$$g_2(\tau) = \frac{\langle I(t)I(t+\tau)\rangle}{\langle I(t)^2\rangle} \tag{1}$$

where, τ is the correlation delay or lag. The Siegert relation [32] establishes the relation between the normalized electric autocorrelation function $g_1(\tau)$ and the normalized light intensity temporal autocorrelation function $g_2(\tau)$,

$$g_2(\tau) = 1 + \beta|g_1(\tau)|^2 \tag{2}$$

where, β is an instrumentation factor that accounts for speckle averaging, light polarization, and laser coherence. In DCS, diffusion of the electric field autocorrelation function is modelled with the Correlation Diffusion Equation, the solution to which for semi-infinite homogeneous tissue geometry is given by,

$$g_1(\tau) = \frac{r_b exp(-K_D(\tau)r_1) - r_1 exp(-K_D(\tau)r_b)}{r_b exp(-K_D(0)r_1) - r_1 exp(-K_D(0)r_b)} \tag{3}$$

where, $K_D\ (\tau)^2 = (\mu_a + 6\mu_s' k_0^2\ F)v/D$, F is the blood flow index to be estimated, $r_1^2 = (l_{tr}^2 + \rho^2)$ and $r_b^2 = ((2z_b + l_{tr})^2 + \rho^2)$ are constants with $l_{tr} = 1/(\mu_a + \mu_s'\ )$,the transport mean-free path, $z_b = (2l_{tr}\ (1 + R_{eff}\ ))/3(1 - R_{eff}\ )$, R_{eff} the effective reflection coefficient that accounts for the refractive index mismatch between the surrounding medium (n_{out}) and tissue (n), μ_a and μ_s', the tissue absorption and reduced scattering coefficients, k_0, the magnitude of the wave vector in tissue, and ρ, the source detector separation.

Biomedical Optics EXPRESS

2.2. Coherence length considerations for DCS light source

Since blood flow contrast in DCS arises from temporal fluctuations in the intensity of the backscattered speckle interference pattern, the coherence length of the laser source (l_c) is an important design consideration. For photon correlation measurements based on quasi-elastic light scattering, the dynamics of intensity fluctuations is a function of flow (dynamic scattering) when l_c is greater than the difference between maximum and minimum photon travel distance in tissue [31,33]. In DCS, the detected speckle pattern is from the coherent addition of an ensemble of light pathlengths. Therefore, the coherence length of DCS light sources should be sufficiently long to account for the spread of light pathlengths from source to detector in tissue, and be greater than the difference between maximum and minimum distance the photon travels inside the tissue [7,31]. While the exact probability distribution of light pathlengths can be estimated for different tissue geometries using analytical [27] or computational methods [34,35], a simpler alternative is to utilize the differential pathlength factor (DPF), which when multiplied by the source detector separation (ρ) yields the average distance travelled by the photon inside tissue [34,36,37]. Delpy et al. [36], measured the DPF to be 5.3 ± 0.3 for rat brain at 783 nm and ~6 for the human brain at 744 nm; DPFs are typically larger for longer wavelengths [36]. Furthermore, the DPF is independent of source-detector separation for ρ>2.5 cm [36]. Accounting for the variation of DPF with wavelength and tissue optical properties, we conservatively suggest that the coherence length of DCS light sources be at least 10~15 times that of the source detector separation. Most practical DCS systems utilize source-detector separations up to 3 cm [8,9,38,39]. Thus, the minimum coherence length of a DCS light source should be 35~50 cm. Note that while most DCS instruments use lasers at a wavelength of 785 nm, these calculations can be readily extended to other wavelengths by use of appropriate values for the DPF.

3. Instrumentation

3.1. Fiber-less laser diode source for DCS (FBDCS)

Considering the coherence requirements of a DCS source, our approach was to build a custom fiber-less laser source (FBDCS) using a single mode diode laser. Figure 1(A) shows a schematic of our FBDCS source. Light from a single mode laser diode (L785P090, Thorlabs, NJ, 785 nm, 90 mW, 5.6 mm TO can package) is collimated with an aspheric lens (355230-B, Thorlabs, NJ; 4.51 mm focal length, 0.55 NA) to yield a 1.5 mm laser beam for use as an illumination source. The laser and lens are aligned and packaged in a custom 3-D printed ABS enclosure (Proto Labs, Inc., USA). The enclosure provides electrical and thermal isolation between the diode and tissue. In our prototype, the diode was driven by current from a standard laser diode controller (LDC205C, Thorlabs, NJ). At typical operating currents (120 mA) we measured the output power of the system to be 65 mW (72% collimation efficiency). Figure 1(B) shows a realized prototype of the FBDCS source, with the laser diode connected to the current controller using a standard ESD protected strain relief cable (SR9C-DB9, Thorlabs, Newton, NJ).

The laser diode was typically operated near its rated operating current (120 mA) without an optical isolator. Therefore, unpredictable laser mode hops can occur due to feedback at optical interfaces during measurements. However, as our DCS measurements below validate, the laser coherence length during the relatively short DCS correlation interval of relevance (typically < 1 ms) is likely to be in excess of ~1 m. To verify the coherence properties of the laser, we measured the optical linewidth of the laser diode, in its intended mode of operation, with scanning Fabry-Perot interferometer (Thorlabs, SA30-73, 1.5 GHz FSR), utilizing 10 ms sweeps of the full spectral range. The spectrum from four measurements were averaged and fit to Lorentzian model [40], to measure a frequency bandwidth of 12.8 MHz (full width half maximum, FWHM), and a spectral bandwidth of $\Delta\lambda = 2.61 \times 10^{-14}\ m$. The coherence length was then calculated as $l_c = \lambda^2/(2 * \pi * \Delta\lambda) = 3.72\ m$, here λ = central wavelength and $\Delta\lambda$ is

Biomedical Optics EXPRESS

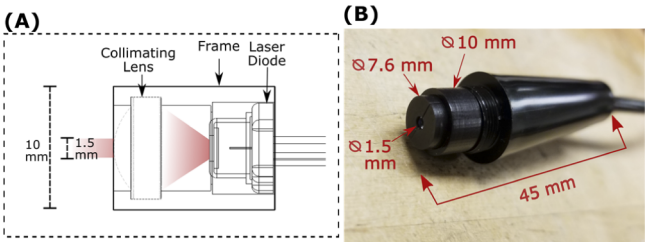

Fig. 1. Fiber-less laser diode source for DCS. (A) Schematic of the Fiber-less laser source (FBDCS) with an optical assembly consisting of a laser diode (L785P090), a collimating lens enclosed within a custom 3D printed enclosure. (B) A prototype showing the FBDCS source with collimation assembly.

optical bandwidth. Thus, selected single mode diode satisfies the coherence requirements for DCS experiments (>50 cm). To further validate that the laser diode is sufficiently coherent within the timescale of our intended DCS experiments, we measured DCS intensity autocorrelation curves from a solid phantom (75019, ISS Inc., $\mu_a = 0.158\ cm^{-1}$ and $\mu_s' = 5.2\ cm^{-1}$ at 690 nm and $\mu_a = 0.154\ cm^{-1}$, $\mu_s' = 4.4 cm^{-1}$ at 830 nm). Light travelling through the solid phantom would experience no dynamic scattering events - thus any decay of the intensity autocorrelation function would be an effect of loss in phase coherence of the source or noise. Figure 2 shows the average intensity autocorrelation curves collected from a solid phantom; data were collected at 5 Hz for 10 min, photon intensity at source-detector separations of 1 cm, 2.5 cm and 3.5 cm were ~500 kHz, ~100 kHz and ~10 kHz respectively. Autocorrelation curves at each SD separation does not decay over the duration of the DCS experiment (0.1 ms). Laser coherence length measurements and experiments on the solid phantom directly and indirectly validate that the selected single mode diode satisfies the coherence requirements for DCS experiments.

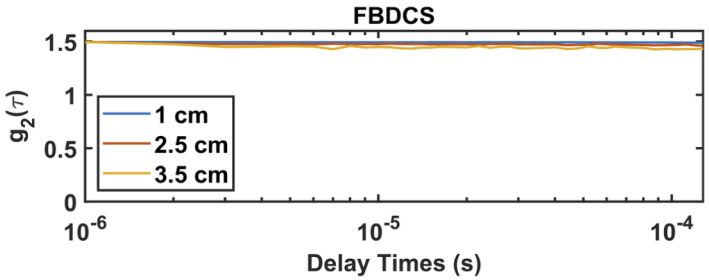

Fig. 2. Plot showing DCS intensity autocorrelation curves ($g_2(\tau)$) acquired from a solid phantom using the FBDCS source at three source-detector separations. The solid phantom had optical properties of $\mu_a = 0.158\ cm^{-1}$ and $\mu_s' = 5.2\ cm^{-1}$ at 690 nm and $\mu_a = 0.154\ cm^{-1}$ and $\mu_s' = 4.4\ cm^{-1}$ at 830 nm. Results shown are an average of 10 min data collected at a frequency of 5 Hz. A total of 3000 autocorrelation functions were averaged.

3.2. *Optical probe and diffuse correlation spectroscopy instrument for validation experiments*

We designed and realized a custom optical probe and DCS instrument to validate the performance of the FBDCS source against a traditional fiber coupled DCS source. Figure 3(A) depicts the schematic of the validation probe with two sources: the red circle denoting the position of the FBDCS source and the red square denoting the position of a multi-mode fiber (GIF625, Fiberoptic Systems Inc, USA). The multi-mode fiber was connected to a traditional fiber coupled

Biomedical Optics EXPRESS

wavelength stabilized source (WSS) (Toptica Photonics, iBeam Smart, 785 nm, 120 mW, l_c>50 m). The probe was configured with three source detector (SD) separations, diagonal distances of 1 cm, 2.5 cm, and 3.5 cm from both sources. At each detector position (denoted by black squares), one or more collocated single mode fibers coupled light to a standard DCS detector (Avalanche photo diode modules, SPCM-AQ4C, Excelitas). Both source and detection fibers were affixed to a prism at the proximal end for ease of light-tissue coupling. DCS autocorrelation functions were computed from all detectors simultaneously using a custom software correlator [17]. Autocorrelation functions derived from the same source-detector position were averaged. Experiments were performed by sequentially illuminating the tissue with the two sources.

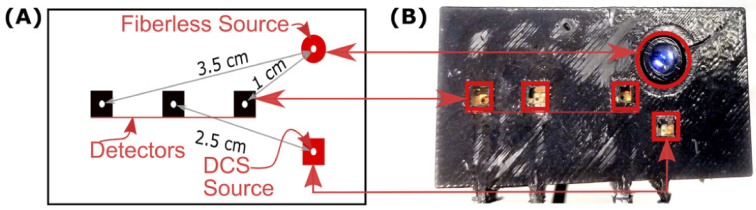

Fig. 3. Custom optical probe used in validation experiments. (A) Schematic of the validation probe consisting of the fiber-less DCS source (red circle) and traditional wavelength stabilized fiber coupled DCS source (red square) at equal distances from three DCS detector fibers (black squares) placed 1 cm, 2.5 cm, and 3.5 cm away. (B) A prototype of the experimental validation probe incorporating the laser source and detector fibers.

Figure 3(B) depicts a realized prototype of the validation probe manufactured by methods described elsewhere [41]. Briefly, prism coupled single (for detectors) and multi-mode (for WSS source) fibers along with the FBDCS source were placed per the schematic in a custom 3D printed mold (RenShape SL 7820, Proto Labs, Inc., USA). A two-part silicone elastomer (VytaFlex, Smooth-On, USA) was mixed with carbon black (JAC-JPX1640, Jacquard,USA) and poured into the mold and cured for 12 hours to realize the validation probe.

4. Experiments and results

4.1. *Blood flow index (BFI) estimated using the FBDCS source is comparable to a wavelength stabilized laser in a tissue simulating phantom*

We first demonstrate that the FBDCS source can measure DCS intensity autocorrelation functions at multiple source-detector separations and validate the blood flow indices (BFI) estimated using the FBDCS as the light source by comparison to traditional DCS sources. The optical probe (Fig. 3) was used to measure intensity autocorrelation functions from a tissue simulating liquid phantom. The liquid phantom was prepared from Intralipid (20% emulsion, Sigma-Aldrich, MO), India ink and distilled water, to realize a sample with absorption coefficient $\mu_a = 0.1\,cm^{-1}$ and reduced scattering coefficient $\mu_s' = 10\,cm^{-1}$ at 785 nm. DCS intensity autocorrelation functions were recorded from both sources (FBDCS and WSS) asynchronously for 120 seconds each, at an acquisition frequency of 10 Hz. A blood flow index (F) was computed by fitting the measured intensity autocorrelation functions to the solution of CDE in Eq. (3). The measurements were performed at room temperature.

Figure 4 displays representative DCS intensity autocorrelation functions measured from the liquid phantom at three source-detector separations, $\rho = 1\ cm$ (blue curve), 2.5 cm (red curve), and 3.5 cm (green curve). These curves are a 50-frame average of intensity autocorrelation functions measured at 10 Hz. The average photon intensity was 490 kHz, 43 kHz, and 4 kHz at each source-detector separation, respectively. An exponential decay of the intensity

Biomedical Optics EXPRESS

autocorrelation function is observed, typical of Brownian motion of fat particles in the intralipid. Notably, these curves were comparable to those measured with the WSS.

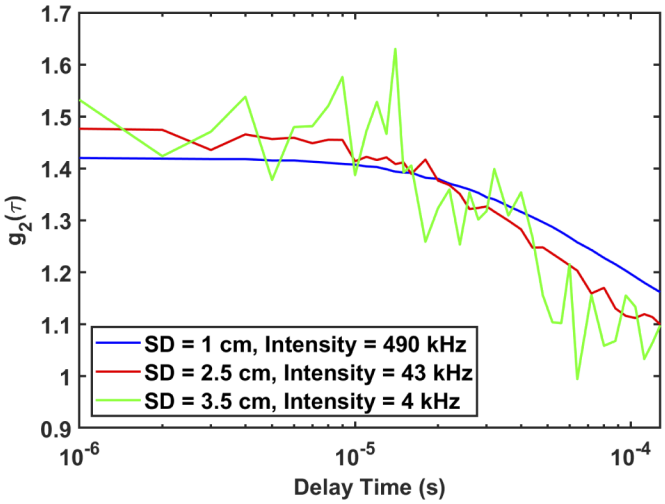

Fig. 4. Representative DCS intensity autocorrelation functions recorded using the fiber-less laser diode source (FBDCS) from a tissue simulating liquid phantom at source detector separations of 1 cm (blue curve), 2.5 cm (red curve) and 3.5 cm (green curve). Autocorrelation curves were recorded at 10 Hz. Each curve is an average of 50 temporal frames with each frame corresponding to DCS photon count acquisition over 100 ms.

Figure 5 displays the estimated blood flow indices from the liquid phantom for each source. Figures 5(B), 5(D) and 5(F) show the time courses of the flow index over the duration of the experiment at source detector separations of $\rho = 1\ cm$, $2.5\ cm$ and $3.5\ cm$ respectively. In each plot, the flow index measured by the FBDCS source is indicated by the red curve, while those measured with WSS is in blue. The curves have been smoothed with a 20-frame moving average filter. At all three source-detector separations, the flow indices measured by the FBDCS compares favorably with those measured with the WSS, highlighting that a fiber-less diode laser source can accurately and quantitatively estimate blood flow. A more quantitative comparison of the respective blood flow indices is depicted in the scatter plots in Figs. 5(A), 5(C) and 5(E). Here, the blood flow index measured with the FBDCS source is plotted along the x-axis, while those measured with the WSS are along the y-axis. The distribution of flow indices are symmetric about the mean (indicated by the dashed red lines) in both directions, indicating good one-to-one agreement between the sources. Table 1 summarizes the mean and standard deviation of flow indices estimated from the liquid phantom using both fiber-less (FBDCS) and wavelength stabilized sources (WSS). A two-sided two-sample ttest (MATLAB, Mathworks, USA) revealed no statistically significant difference in the mean flow measured by the two sources ($p>0.05$) for 1 and 2.5 cm source detector separation. Statistical testing was not reliable for measurements at 3.5 cm due to higher incidence of noise. Note that the measurements are noisier at longer source-detector separations (both sources) because of a decrease in measured photon intensity. The differences in estimated blood flow index at 3.5 cm source detector separation could be due to the FBDCS source having slightly wider illumination area than the wavelength stabilized source. As a result, the FBDCS source could appear to be an extended illumination source rather than a point source (as assumed by the analysis models). This mismatch could cause estimates of blood flow index to deviate slightly at larger source detector separations.

Biomedical Optics EXPRESS

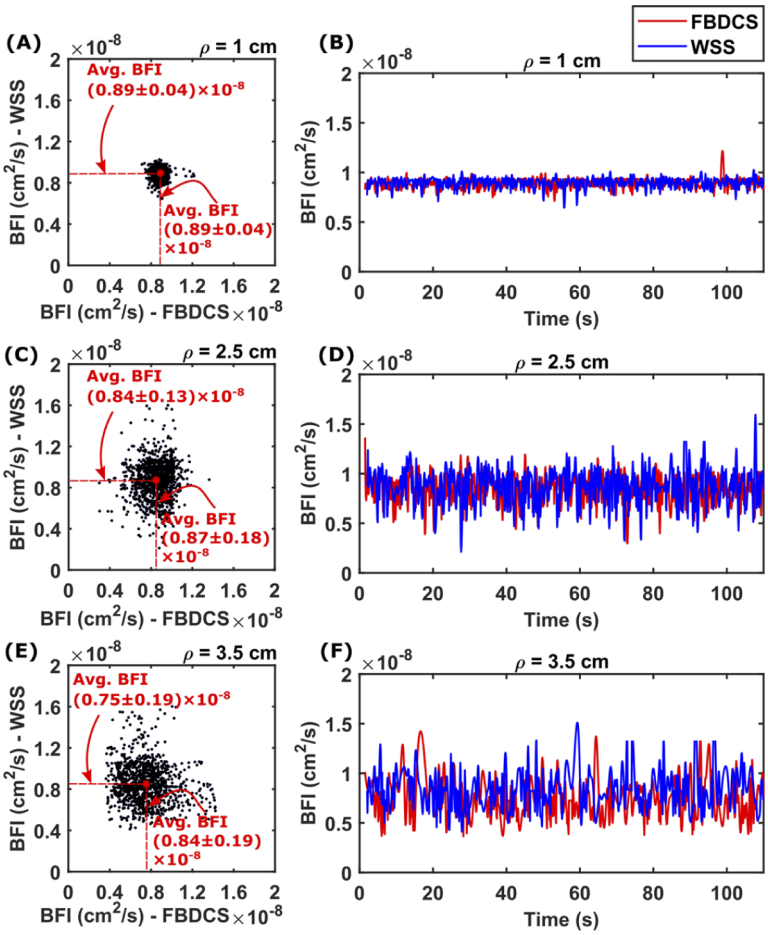

Fig. 5. Comparison of flow measured from tissue simulating phantom using the fiber-less (FBDCS) and wavelength stabilized (WSS) laser sources. Time courses of flow indices measured at source detection separations 1 cm, 2.5 cm and 3.5 cm are shown in (B), (D) and (F) respectively. Panels (A), (C), and (E) show scatter plots comparing the flow measured with one source against the other. The scatter plots highlight that the mean flow measured with the two sources are in good agreement, with symmetrical spreads in flow estimates along both dimensions.

Table 1. Flow indices measured from liquid phantom using both fiber-less (FBDCS) and wavelength stabilized sources (WSS).

Source-detector separation	Flow index F (cm^2/s)	
	FBDCS	WSS
1 cm	$(0.89 \pm 0.04) \times 10^{-8}$	$(0.89 \pm 0.04) \times 10^{-8}$
2.5 cm	$(0.84 \pm 0.13) \times 10^{-8}$	$(0.87 \pm 0.18) \times 10^{-8}$
3.5 cm	$(0.75 \pm 0.19) \times 10^{-8}$	$(0.84 \pm 0.19) \times 10^{-8}$

Biomedical Optics EXPRESS

4.2. Signal-to-noise ratio of intensity autocorrelation function measurements are comparable between FBDCS and WSS

Our second validation experiment concerns the signal-to-noise ratio of intensity autocorrelation functions measured using the fiber-less source (FBDCS). The DCS correlation noise model offers a framework to evaluate the signal-to-noise ratio (SNR) of the measured intensity autocorrelation function as a function of measurement integration time (or measurement speed) and measured photon intensity [42]. Accordingly, we define noise ($\sigma(\tau)$) as the standard deviation of the intensity autocorrelation function $g_2(\tau)$ and SNR($\zeta(\tau)$) as $\zeta(\tau) = (g_2(\tau) - 1)/\sigma(\tau)$. DCS intensity autocorrelation functions were recorded from the tissue simulating liquid phantom with the fiber-less DCS source, at source detector separation of 1 cm. In separate measurements, the optical power of the laser was varied to effect a measured photon count rate of $30kHz$, $100kHz$ and $300kHz$. At each power level, intensity autocorrelation functions were recorded at different integration times ranging from $1ms$ to $100ms$. Figure 6 shows the noise and SNR of the measurements for 20 μs and 40 μs delay times. Figure 6(A) shows the representative decrease in variability of $g_2(\tau)$ with increasing integration time at delay time of $20\mu s$. Figures 6(B) and 6(C) show the noise and SNR of the $g_2(\tau)$ measurements at $\tau = 20\mu s$ respectively; Figs. 6(D)

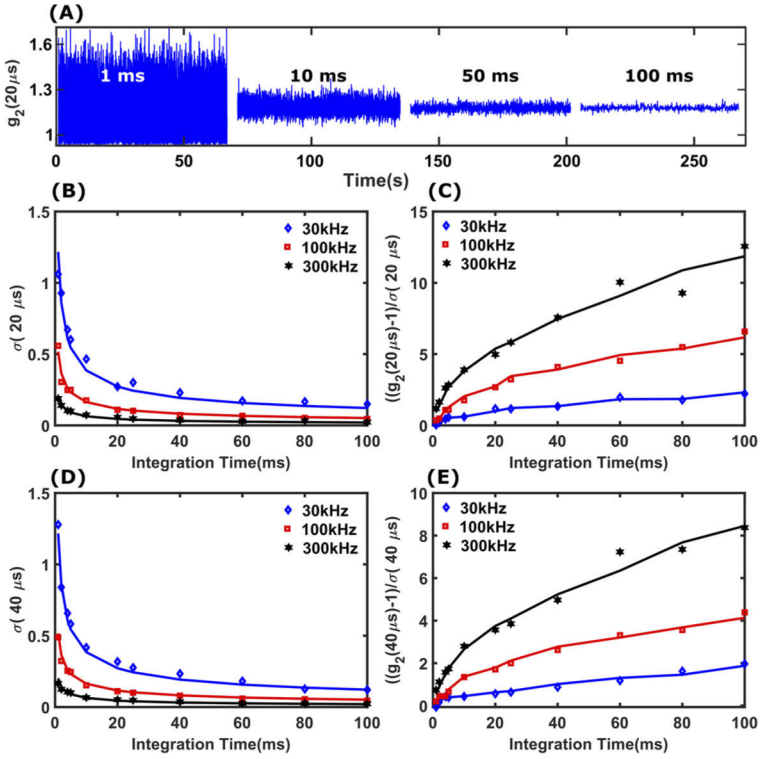

Fig. 6. Experimental measurement of signal-to-noise ratio of DCS intensity autocorrelation functions with the fiber-less DCS (FBDCS) source. (A) Representative fluctuation of the measured autocorrelation function at delay time 20 μs for integration times 1ms, 10ms, 50ms and 100ms. Longer integration time increases the averaging of measurements and reduces noise. (B) and (D) Noise in measurement of $g_2(\tau)$ for delay times 20 μs and 40 μs respectively. (C) and (E) SNR of $g_2(\tau)$ measurements for delay times 20 μs and 40 μs respectively. The noise and SNR estimates for photon count rates of 30 kHz, 100 kHz and 300 kHz are marked with blue, red and black markers respectively, while the corresponding solid lines are fits to a DCS correlation noise model.

Biomedical Optics EXPRESS

and 6(E) show the corresponding curves for $\tau = 40\mu s$. In each panel, measurements at $30kHz$, $100kHz$ and $300kHz$ are indicated by blue, red and black markers, while the solid blue, red and black lines are fits to a DCS correlation noise model [42]. As expected, the noise of correlation measurements decreases (and SNR increases) with increase in integration time and photon count rate. At $30kHz$ photon count rates, a SNR of 1 is achieved at integration times of 20 ms for $\sigma = 20\ \mu s$ and 40 ms for $\sigma = 40\ \mu s$. These results are similar to those obtained with standard DCS instruments [17,42].

Figure 7 compares the noise and SNR of $g_2(\tau)$ measurements obtained with FBDCS and WSS sources. Noise and SNR were estimated from sequential measurements of $g_2(\tau)$ with the FBDCS and WSS source, with source optical powers varied to effect a $100\,kHz$ photon count rate at the detector (source-detector separation of 1 cm). Figure 7(A) and 7(B) displays a plot of noise and SNR of $g_2(\tau)$ at $\tau = 20\mu s$; data from the FBDCS/WSS source is indicated with red/blue markers respectively, while the solid lines represent fits to a DCS correlation noise model. The noise and SNR measured with the two sources are remarkably similar, with the FBDCS source showing marginally higher noise at lower integration times.

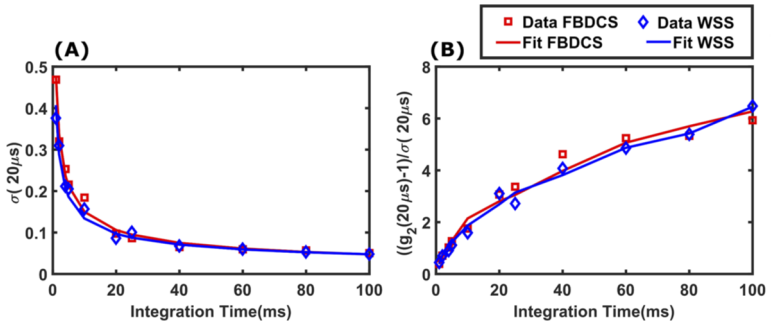

Fig. 7. Comparison of noise (A) and signal-to-noise ratio (B) of DCS intensity autocorrelation functions measured using the fiber-less source (FBDCS, red markers) and the wavelength stabilized source (WSS, blue markers). Solid lines are fits to a DCS correlation noise model [37].

4.3. *Blood flow dynamics measured in-vivo with FBDCS is comparable to those measured with WSS*

Finally, we characterized the ability of the fiber-less DCS source (FBDCS) to measure blood flow dynamics *in-vivo* and validated it by comparison with a wavelength stabilized source (WSS). We measured deep tissue changes in blood flow in the arm of a healthy volunteer during an arm-cuff occlusion study. All experimental protocols were approved by the Institutional Review Board at the University of South Florida. Figure 8 shows the experiment setup. Briefly, the validation probe (Fig. 3) was placed on the forearm of a healthy volunteer. A blood pressure cuff, connected to a tourniquet system (A.T.S. 4000, Zimmer, USA), was placed around the bicep and used to produce transient cuff ischemia. The validation probe was connected to a standard DCS instrument as described earlier. The cuff-occlusion protocol consisted of a 2-minute baseline, followed by a 1-minute cuff ischemia where the blood pressure cuff was inflated to 200mmHg, and finally a 2-minute post occlusion recovery. The protocol was repeated twice, with tissue being illuminated by FBDCS in the first trial and the Wavelength Stabilized Source (WSS) in the second. A 10-minute resting period between trials was observed to restore the arm blood flow to baseline. DCS intensity autocorrelation functions were recorded at 10 Hz and were fit to Eq. (3) to derive estimates of blood flow. The source power of both the lasers (FBDCS and WSS) were

Biomedical Optics EXPRESS

adjusted to illuminate the tissue with 50 mW optical power; this yielded an average photon count rate of 700, 45 and 6 KHz at 1, 2.5 and 3.5 cm source-detector separations respectively.

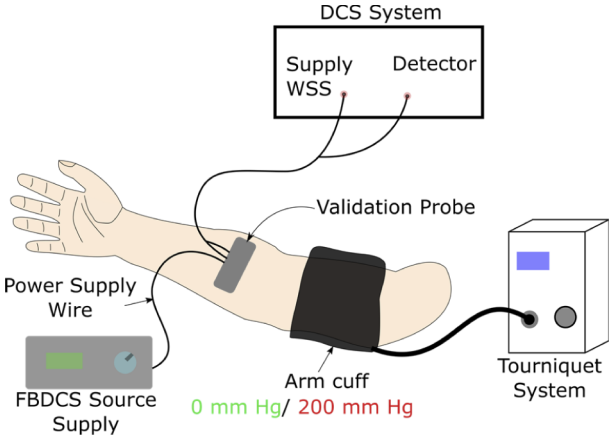

Fig. 8. Schematic illustrating the *in-vivo* cuff-occlusion experiment. The validation probe (Fig. 3) was placed on the forearm of a volunteer, with the detectors centered on the radial artery and two sources illuminating the artery from either side. The distal end of the validation probe was connected to a standard DCS instrument. An arm cuff (connected to a tourniquet system) was wrapped around the bicep to effect transient cuff-ischemia.

Figure 9 shows representative 20 second time course of forearm blood flow measured at baseline using the fiber-less source. Blood flow pulsatility is observed in measurements at both 1 cm (blue curves) and 2.5 cm (red curves); waveform features similar to an ECG-QRS peak along with the dicrotic notch is clearly resolved. These results are similar to previous pulsatile

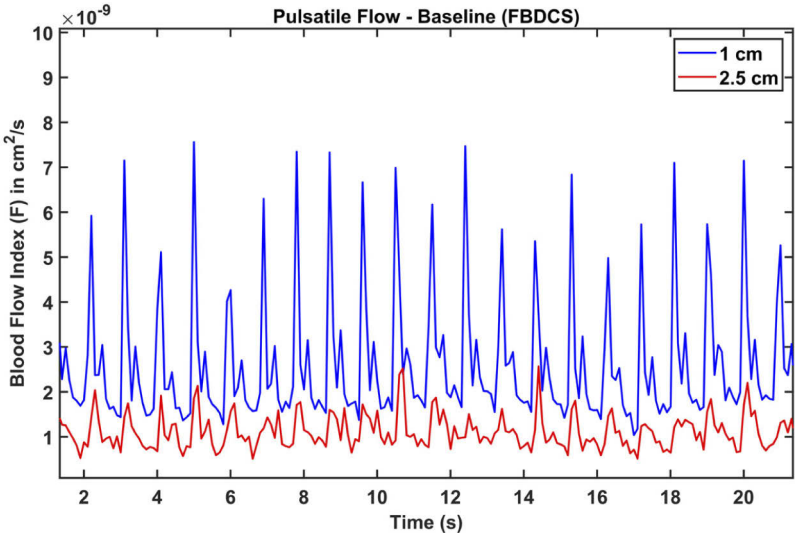

Fig. 9. Representative time courses of pulsatile blood flow (baseline) measured on a subject's forearm using the fiber-less DCS source. Flow data was acquired at 10 Hz. Blood flow pulsatility was observed at both the 1 cm (blue) and 2.5 cm (red) source-detector separations.

Biomedical Optics EXPRESS

arm blood flow [17,43] measured with traditional fast DCS instruments and serves to highlight the sensitivity of the FBDCS source to dynamic blood flow changes *in* vivo.

Figure 10 shows the blood flow dynamics measured due to the cuff-occlusion experiment. Here, the blood flow time courses have been smoothed with a 20-frame moving average filter. Figures 10(A), (C) and (E) show the measured blood flow at 1, 2.5 and 3.5 cm source-detector separations, while Figs. 10(B), (D) and (F) show the respective relative blood flow changes. In all panels, blood flow measured with the FBDCS source is depicted in red, while those measured with the WSS source is in blue. Two black vertical lines denote the occlusion period. Flow measurements realized by the FBDCS source accurately track a nearly 100% reduction in blood flow due to cuff-occlusion and a transient hyperemic response. These results are similar to those obtained in similar studies, as well as the comparison flow changes measured with the WSS source on the validation probe. Minor deviations may be explained by the two sources sampling slightly different tissue volumes. Note that the cuff-occlusion and hyperemic response is resolved at the 3.5 cm source-detector separation despite the significant noise presence.

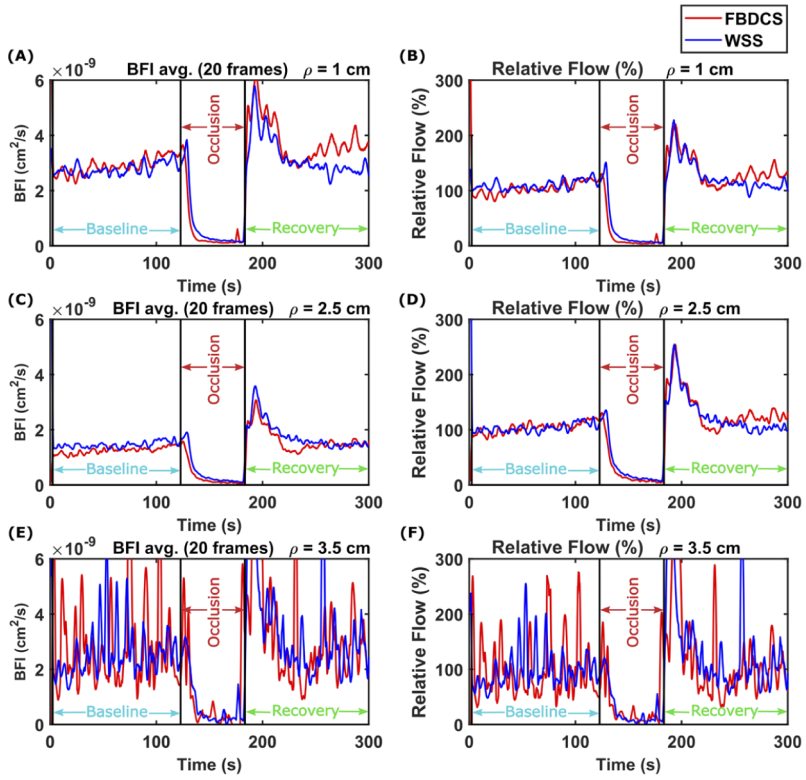

Fig. 10. Blood flow dynamics due to *in-vivo* arm cuff occlusion. Panels (A), (C) and (E) show the time courses of blood flow measured source-detector separation of 1 cm, 2.5 cm, and 3.5 cm; panels (B), (D) and (F) show the corresponding relative blood flow changes. In all panels, red lines indicate measurements with the fiber-less DCS source, blue lines indicate measurements with the wavelength stabilized source and vertical black lines indicate occlusion period. The flow indices at SD separation 3.5 cm are noisy due to low photon count rates (both sources). Minor deviations in the flow measured by the two sources can be attributed to the positional difference of the sources relative to the radial artery and asynchronous acquisition.

Biomedical Optics EXPRESS

5. Discussion

Traditionally, DCS instruments have used laser sources with very high coherence length, in part to compensate for light travelling through multiple pathlengths in long fiber optic cables. While these wavelength stabilized laser diode modules are relatively easy to use (often fiber-coupled and 'turnkey'), they can be bulky and expensive. In this contribution, we have demonstrated that DCS blood flow measurements can be reliably and accurately performed with a low coherence length (less than 5 m), off-the-shelf, single mode diode laser. While these are not the first DCS measurements with low-coherence light source, to our knowledge, this is the first time such lasers have been rigorously tested and validated for DCS blood flow measurements. By direct comparisons to fiber-coupled long coherence length wavelength stabilized lasers, we show that our implementation of a fiber-less source (a) is accurate in estimating DCS blood flow indices at source-detector separations of up to 3.5 cm, (b) measures DCS intensity autocorrelation functions at signal-to-noise ratios comparable to wavelength stabilized sources, and (c) can measure dynamic changes in blood flow in humans. The performance of the two sources is nearly identical for source-detector separations of 1 and 2.5 cm, but deviate slightly at 3.5 cm. This is primarily due to the significantly reduced photon intensity and subsequent increase in noise. When corrected for signal intensity, the signal-to-noise ratio of both sources are identical. We also note that the FBDCS assembly has a height of ~30 mm and width of ~50 mm but weighs only around ~50 gm (slightly heavier than that of a traditional DCS probe). The weight of the FBDCS source is not high enough where pressure from the probe will cause restrictions to blood flow in tissue. Furthermore, in a standalone FBDCS setup (i.e., without validation DCS probes present) the size and weight can be reduced to similar level of a DCS probe.

A few prior studies have utilized fiber-less designs for DCS blood flow measurements, using both traditional long coherence length lasers as well as low-coherence diodes. Lin et. al. reported the development of a dual-wavelength non-contact DCS flow-oximeter system [44,45], where the laser source was collimated and projected to the tissue surface via a scanning mechanism. While these systems did not use fibers to illuminate the tissue, they still utilized long coherence length lasers. Furthermore, the scanning mechanism and lens system resulted in a large/bulky system. By contrast, our approach features a smaller, portable, wearable laser source for DCS blood flow measurements. Huang et. al. [22], and Liu et. al. [46] have utilized low-coherence length (<1 m) off-the shelf laser diodes for wearable blood flow measurements with DCS instruments based on diffuse speckle contrast analysis. In these implementations, the laser diode was coupled directly to the skin without use of collimation lenses. Notably, these experiments were limited to source-detector separations of less than 2 cm, and they did not directly compare DCS intensity autocorrelation measurements with traditional DCS sources and detectors.

Our approach directly couples light into tissue via a collimation lens placed in front of the laser diode. The use of a collimation lens is critical because the natural divergence of laser diodes is typically too high to yield measurable signal at the detector, especially at large source detector separations. Furthermore, when operated at operating powers of ~100 mW, the heat generated in the laser diodes may cause thermal tissue damage. Therefore, continuous real-time monitoring of flow with these sources would require efficient thermal isolation between the laser diode and tissue surface. The designed collimation setup efficiently provides this thermal and electrical isolation, thereby permitting operation at higher optical powers. As a result of these design choices, our FBDCS source can measure blood flow at 3.5 cm source detector separation and is safer for use on clinical populations. We note that the width of the collimated beam may result in an extended-source illumination, rather than point-source illumination, leading to speckle averaging at the detector and reduced β. Therefore, narrow beam diameters are preferable provided the laser irradiation is within ANSI limits [47]. Since the collimation system provides electrical and thermal protection, care should be observed to use appropriate materials in fabrication of these components.

Biomedical Optics EXPRESS

There are several advantages to using a fiber-less diode source for DCS blood flow measurements. First, it greatly simplifies instrument design and can reduce the cost of DCS sources by as much as 100-fold. Indeed, our approach brings DCS sources to the cost and accessibility of commercial Near Infrared Spectroscopy devices. Second, since the design of the source greatly reduces coherence requirements, it can be readily adapted to perform DCS blood flow measurements at longer wavelengths (e.g., 1064 nm [39]), where wavelength stabilized sources may be cost- and technologically restrictive. Third, cost and size advantages of the fiber-less source makes it an attractive alternative for large scale Diffuse Correlation Tomography experiments to *image* blood flow in tissue. Furthermore, the fiber-less source can be readily incorporated with newer speckle contrast-based detection technologies to effect portable/wearable deep tissue blood flow monitors.

6. Conclusion

We have reported the development of a fiber less, low power laser source capable for deep tissue blood flow measurements with DCS. We have validated this new laser source against gold-standard, state-of-the-art fiber-coupled wavelength stabilized lasers typically used in DCS instruments. Our results show that the fiber-less DCS source can quantitatively measure blood flow at signal-to-noise ratios that are comparable to traditional DCS sources. The development of this low-cost DCS light source will greatly simplify DCS blood flow instruments and will pave the way for wearable deep-tissue blood flow monitors.

Funding. University of South Florida; Southeastern Center for Electrical Engineering Education (SCEEE) (Research Initiation Award); National Institute of General Medical Sciences (R21GM137209).

Acknowledgements. We thank Wesley Baker for the help with liquid phantom preparation and Abdul Mohaimen Safi for help with the Fabry–Pérot measurement.

Disclosures. AB (P), ABP: Spkl LLC (I, P)

Data availability. Data underlying the results presented in this paper are not publicly available at this time but may be obtained from the authors upon reasonable request.

References

1. T. Durduran, C. Zhou, B. L. Edlow, G. Yu, R. Choe, M. N. Kim, B. L. Cucchiara, M. E. Putt, Q. Shah, S. E. Kasner, J. H. Greenberg, A. G. Yodh, and J. A. Detre, "Transcranial optical monitoring of cerebrovascular hemodynamics in acute stroke patients," Opt. Express **17**(5), 3884–3902 (2009).
2. C. G. Favilla, A. B. Parthasarathy, J. A. Detre, A. G. Yodh, M. T. Mullen, S. E. Kasner, K. Gannon, and S. R. Messé, "Non-invasive respiratory impedance enhances cerebral perfusion in healthy adults," Front. Neurol. **8**, 45 (2017).
3. V. Jain, E. M. Buckley, D. J. Licht, J. M. Lynch, P. J. Schwab, M. Y. Naim, N. A. Lavin, S. C. Nicolson, L. M. Montenegro, A. G. Yodh, and F. W. Wehrli, "Cerebral oxygen metabolism in neonates with congenital heart disease quantified by MRI and optics," J. Cereb. Blood Flow Metab. **34**(3), 380–388 (2014).
4. G. Yu, T. Durduran, G. Lech, C. Zhou, B. Chance, E. R. Mohler, and A. G. Yodh, "Time-dependent blood flow and oxygenation in human skeletal muscles measured with noninvasive near-infrared diffuse optical spectroscopies," J. Biomed. Opt. **10**(2), 024027 (2005).
5. N. A. Lassen and M. S. Christensen, "Physiology of cerebral blood flow," Br. J. Anaesth. **48**(8), 719–734 (1976).
6. S. Strandgaard and O. B. Paulson, "Regulation of cerebral blood flow in health and disease," Journal of Cardiovascular Pharmacology **19**, S89–S93 (1992).
7. D. A. Boas and A. G. Yodh, "Spatially varying dynamical properties of turbid media probed with diffusing temporal light correlation," J. Opt. Soc. Am. A **14**(1), 192 (1997).
8. T. Durduran and A. G. Yodh, "Diffuse correlation spectroscopy for non-invasive, micro-vascular cerebral blood flow measurement," NeuroImage **85**, 51–63 (2014).
9. E. M. Buckley, A. B. Parthasarathy, P. E. Grant, A. G. Yodh, and M. A. Franceschini, "Diffuse correlation spectroscopy for measurement of cerebral blood flow: future prospects," Neurophotonics **1**(1), 011009 (2014).
10. G. Yu, T. F. Floyd, T. Durduran, C. Zhou, J. Wang, J. A. Detre, and A. G. Yodh, "Validation of diffuse correlation spectroscopy for muscle blood flow with concurrent arterial spin labeled perfusion MRI," Opt. Express **15**(3), 1064–1075 (2007).
11. S. A. Carp, G. P. Dai, D. A. Boas, M. A. Franceschini, and Y. R. Kim, "Validation of diffuse correlation spectroscopy measurements of rodent cerebral blood flow with simultaneous arterial spin labeling MRI; towards MRI-optical continuous cerebral metabolic monitoring," Biomed. Opt. Express **1**(2), 553 (2010).

Biomedical Optics EXPRESS

12. E. M. Buckley, N. M. Cook, T. Durduran, M. N. Kim, C. Zhou, R. Choe, G. Yu, S. Shultz, C. M. Sehgal, D. J. Licht, P. H. Arger, M. E. Putt, H. Hurt, and A. G. Yodh, "Cerebral hemodynamics in preterm infants during positional intervention measured with diffuse correlation spectroscopy and transcranial Doppler ultrasound," Opt. Express **17**(15), 12571–12581 (2009).
13. E. M. Buckley, D. Hance, T. Pawlowski, J. Lynch, F. B. Wilson, R. C. Mesquita, T. Durduran, L. K. Diaz, M. E. Putt, D. J. Licht, M. A. Fogel, and A. G. Yodh, "Validation of diffuse correlation spectroscopic measurement of cerebral blood flow using phase-encoded velocity mapping magnetic resonance imaging," J. Biomed. Opt. **17**, 037007 (2012).
14. E. M. Buckley, J. M. Lynch, D. A. Goff, P. J. Schwab, W. B. Baker, T. Durduran, D. R. Busch, S. C. Nicolson, L. M. Montenegro, M. Y. Naim, R. Xiao, T. L. Spray, A. G. Yodh, J. W. Gaynor, and D. J. Licht, "Early postoperative changes in cerebral oxygen metabolism following neonatal cardiac surgery: Effects of surgical duration," J. Thorac. Cardiovasc. Surg. **145**(1), 196–205.e1 (2013).
15. A. S. Kogler, T. V. Bilfinger, R. M. Galler, R. C. Mesquita, M. Cutrone, S. S. Schenkel, A. G. Yodh, and T. F. Floyd, "Fiber-optic monitoring of spinal cord hemodynamics in experimental aortic occlusion," Anesthesiology **123**(6), 1362–1373 (2015).
16. R. C. Mesquita, A. D'Souza, T. V. Bilfinger, R. M. Galler, A. Emanuel, S. S. Schenkel, A. G. Yodh, and T. F. Floyd, "Optical Monitoring and Detection of Spinal Cord Ischemia," PLoS One **8**(12), e83370 (2013).
17. D. Wang, A. B. Parthasarathy, W. B. Baker, K. Gannon, V. Kavuri, T. Ko, S. Schenkel, Z. Li, Z. Li, M. T. Mullen, J. A. Detre, and A. G. Yodh, "Fast blood flow monitoring in deep tissues with real-time software correlators," Biomed. Opt. Express **7**(3), 776–797 (2016).
18. D. Magatti and F. Ferri, "Fast multi-tau real-time software correlator for dynamic light scattering," Appl. Opt. **40**(24), 4011 (2001).
19. W. Lin, D. R. Busch, C. C. Goh, J. Barsi, and T. F. Floyd, "Diffuse correlation spectroscopy analysis implemented on a field programmable gate array," IEEE Access **7**, 122503–122512 (2019).
20. A. Biswas, D. A. Buffone, and A. B. Parthasarathy, "Fast diffuse correlation spectroscopy with low-cost microcontroller," in *Biophotonics Congress: Biomedical Optics Congress 2018 (Microscopy/Translational/Brain/OTS)* (OSA, 2018), p. JW3A.20.
21. R. Bi, J. Dong, and K. Lee, "Deep tissue flowmetry based on diffuse speckle contrast analysis," Opt. Lett. **38**(9), 1401–1403 (2013).
22. C. Huang, M. Seong, J. P. Morgan, S. Mazdeyasna, J. G. Kim, J. T. Hastings, and G. Yu, "Low-cost compact diffuse speckle contrast flowmeter using small laser diode and bare charge-coupled-device," J. Biomed. Opt. **21**, 080501 (2016).
23. J. Liu, H. Zhang, J. Lu, X. Ni, and Z. Shen, "Quantitative model of diffuse speckle contrast analysis for flow measurement," J. Biomed. Opt. **22**(7), 076016 (2017).
24. T. Dragojević, J. L. Hollmann, D. Tamborini, D. Portaluppi, M. Buttafava, J. P. Culver, F. Villa, and T. Durduran, "Compact, multi-exposure speckle contrast optical spectroscopy (SCOS) device for measuring deep tissue blood flow," Biomed. Opt. Express **9**(1), 322–334 (2018).
25. A. Biswas and A. B. Parthasarathy, "Fast, compact measurement of deep tissue blood flow with integrated diffuse correlation spectroscopy," in *Biomedical Applications of Light Scattering X*, A. Wax and V. Backman, eds. (SPIE, 2020), p. 32.
26. A. Biswas and A. B. Parthasarathy, "An integrated detection scheme for fast, embedded measurement of deep tissue blood flow with Diffuse Correlation Spectroscopy," in *Biophotonics Congress: Biomedical Optics 2020 (Translational, Microscopy, OCT, OTS, BRAIN) (2020), Paper SM3D.5* (Optical Society of America, 2020), p. SM3D.5.
27. T. Durduran, R. Choe, W. B. Baker, and A. G. Yodh, "Diffuse optics for tissue monitoring and tomography," Rep. Prog. Phys. **73**(7), 076701 (2010).
28. G. Maret and P. E. Wolf, "Multiple light scattering from disordered media. The effect of Brownian motion of scatterers," Z. Physik B - Condensed Matter **65**(4), 409–413 (1987).
29. M. P. V. Albada and A. Lagendijk, "Observation of Weak Localization of Light in a Random Medium," Phys. Rev. Lett. **55**(24), 2692–2695 (1985).
30. D. J. Pine, D. A. Weitz, J. X. Zhu, and E. Herbolzheimer, "Diffusing-wave spectroscopy: dynamic light scattering in the multiple scattering limit," J. Phys. **51**(18), 2101–2127 (1990).
31. T. Bellini, M. A. Glaser, N. A. Clark, and V. Degiorgio, "Effects of finite laser coherence in quasielastic multiple scattering," Phys. Rev. A **44**(8), 5215–5223 (1991).
32. P.-A. Lemieux and D. J. Durian, "Investigating non-Gaussian scattering processes by using nth -order intensity correlation functions," J. Opt. Soc. Am. A **16**(7), 1651 (1999).
33. P. N. Pusey, J. M. Vaughan, and D. V. Willetts, "Effect of spatial incoherence of the laser in photon-correlation spectroscopy," J. Opt. Soc. Am. **73**(8), 1012 (1983).
34. M. Hiraoka, M. Firbank, M. Essenpreis, M. Cope, S. R. Arridge, P. van der Zee, and D. T. Delpy, "A Monte Carlo investigation of optical pathlength in inhomogeneous tissue and its application to near-infrared spectroscopy," Phys. Med. Biol. **38**(12), 1859–1876 (1993).
35. H. Dehghani, M. E. Eames, P. K. Yalavarthy, S. C. Davis, S. Srinivasan, C. M. Carpenter, B. W. Pogue, and K. D. Paulsen, "Near infrared optical tomography using NIRFAST: algorithm for numerical model and image reconstruction," Commun. Numer. Methods Eng. **25**(6), 711–732 (2009).

Biomedical Optics EXPRESS

36. D. T. Delpy, M. Cope, P. van der Zee, S. Arridge, S. Wray, and J. Wyatt, "Estimation of optical pathlength through tissue from direct time of flight measurement," Phys. Med. Biol. **33**(12), 1433–1442 (1988).
37. S. R. Arridge, M. Cope, and D. T. Delpy, "The theoretical basis for the determination of optical pathlengths in tissue: temporal and frequency analysis," Phys. Med. Biol. **37**(7), 1531–1560 (1992).
38. M. N. Kim, T. Durduran, S. Frangos, B. L. Edlow, E. M. Buckley, H. E. Moss, C. Zhou, G. Yu, R. Choe, E. Maloney-Wilensky, R. L. Wolf, M. S. Grady, J. H. Greenberg, J. M. Levine, A. G. Yodh, J. A. Detre, and W. A. Kofke, "Noninvasive measurement of cerebral blood flow and blood oxygenation using near-infrared and diffuse correlation spectroscopies in critically brain-injured adults," Neurocrit. Care **12**(2), 173–180 (2010).
39. S. A. Carp, D. Tamborini, D. Mazumder, K.-C. Wu, M. B. Robinson, K. A. Stephens, O. Shatrovoy, N. Lue, N. Ozana, M. H. Blackwell, and M. A. Franceschini, "Diffuse correlation spectroscopy measurements of blood flow using 1064 nm light," J. Biomed. Opt. **25**, 097003 (2020).
40. N. Balakrishnan and V. B. Nevzorov, "A primer on statistical distributions," 323 (n.d.).
41. W. B. Baker, A. B. Parthasarathy, T. S. Ko, D. R. Busch, K. Abramson, S.-Y. Tzeng, R. C. Mesquita, T. Durduran, J. H. Greenberg, D. K. Kung, and A. G. Yodh, "Pressure modulation algorithm to separate cerebral hemodynamic signals from extracerebral artifacts," Neurophotonics **2**(3), 035004 (2015).
42. C. Zhou, G. Yu, D. Furuya, J. H. Greenberg, A. G. Yodh, and T. Durduran, "Diffuse optical correlation tomography of cerebral blood flow during cortical spreading depression in rat brain," Opt. Express **14**(3), 1125 (2006).
43. Z. Li, W. B. Baker, A. B. Parthasarathy, T. S. Ko, D. Wang, S. Schenkel, T. Durduran, G. Li, and A. G. Yodh, "Calibration of diffuse correlation spectroscopy blood flow index with venous-occlusion diffuse optical spectroscopy in skeletal muscle," J. Biomed. Opt. **20**(12), 125005 (2015).
44. Y. Lin, L. He, Y. Shang, and G. Yu, "Noncontact diffuse correlation spectroscopy for noninvasive deep tissue blood flow measurement," J. Biomed. Opt. **17**, 010502 (2012).
45. T. Li, Y. Lin, Y. Shang, L. He, C. Huang, M. Szabunio, and G. Yu, "Simultaneous measurement of deep tissue blood flow and oxygenation using noncontact diffuse correlation spectroscopy flow-oximeter," Sci. Rep. **3**(1), 1358 (2013).
46. X. Liu, Y. Gu, C. Huang, M. Zhao, Y. Cheng, E. G. A. Jawdeh, H. S. Bada, L. Chen, and G. Yu, "Simultaneous measurements of tissue blood flow and oxygenation using a wearable fiber-free optical sensor," J. Biomed. Opt. **26**, 012705 (2021).
47. D. C. Winburn, *Practical Laser Safety*, 2nd ed., rev.expanded, Occupational Safety and Health No. 11 (M. Dekker, 1990).